IEEE Access
Multidisciplinary ⋮ Rapid Review ⋮ Open Access Journal

Received October 5, 2021, accepted December 3, 2021, date of publication December 13, 2021, date of current version December 22, 2021.

Digital Object Identifier 10.1109/ACCESS.2021.3135035

Development of a Compact Pneumatic Valve Using Rotational Motion for a Pneumatically Driven Mobile Robot With Periodic Motion in a Pipe

HIROTO SATO[1], KOUSUKE UCHIYAMA[1], YUKI MANO[1], FUMIO ITO[1], (Graduate Student Member, IEEE), SHUNICHI KURUMAYA[1], MANABU OKUI[1], (Member, IEEE), YASUYUKI YAMADA[2], (Member, IEEE), AND TARO NAKAMURA[1], (Member, IEEE)

[1]Department of Precision Mechanics, Faculty of Science and Engineering, Chuo University, Bunkyo-ku 112-8551, Japan
[2]Department of System Design Engineering, Faculty of Design Engineering, Hosei University, Tokyo 102-8160, Japan

Corresponding author: Hiroto Sato (h_sato@bio.mech.chuo-u.ac.jp)

This work was supported in part by the Gesuido Academic Incubation to Advanced (GAIA) Project of the Ministry of Land, Infrastructure, Transport and Tourism, Japan.

ABSTRACT This paper describes the development of a compact pneumatic valve that can obtain a high flow rate in a periodically pneumatically driven pipe-moving robot. Plumbing facilities around the world have fallen into disrepair in recent years. Pneumatically driven mobile robots are widely used as an inspection method due to the small inner diameter and complicated shape of the pipes. Various types of robots have been studied, such as earthworm, inchworm, and spiral tube robots. However, these robots are driven by existing pneumatic valve technologies, such as needle-type and solenoid valves, which limit the use of small mobile robots. Small pneumatic valves have a low flow rate, and the entire system is complicated because multiple air pressures are controlled by multiple electrical systems. Thus, focusing on the structure and periodic motion of the ball valve, we developed a pneumatic valve that can periodically apply pressure to multiple pneumatic actuators using only rotational motion with one degree of freedom. We also applied this pneumatic valve to a wave propagation robot and discussed the theoretical running speed of the robot with this valve.

INDEX TERMS Pneumatic, periodic air supply, mobile robot, pipe inspection.

I. INTRODUCTION

Plumbing facilities are declining worldwide [1]. Many of these aging plumbing systems are left unattended, and facility managers are not even aware of their aging. These decrepit conditions have led to accidents such as gas leaks from plumbing systems and road collapses caused by burst water pipes. To prevent these accidents, periodic inspection of the pipes is required to find the damaged parts and replace them efficiently, as regular replacement of the pipes is expensive [2]. There are two types of inspection methods for pipelines: pipe extraction and nondestructive inspection. In the pipe extraction method, pipes buried underground are excavated, removed, and reinstalled after inspection. Because this method requires considerable time and cost, and may damage the pipe during excavation, non-destructive inspection is recommended [3]. A push-in endoscope is widely used in non-destructive inspections. This device has a simple structure with a camera at the tip and wiring at the rear. During inspection, the operator pushes the wires to allow the camera to penetrate further into the pipe. However, the method using a push-in type endoscope is not suitable for inspection of pipes that are very long and have small diameters (for example, in Japan, maintenance hatches for external inspection equipment are available about every 100 m in sewer pipes, and the inner diameter of the pipe is less than 150 mm.) It is challenging to inspect long-distance pipes with small diameters. When a push-in endoscope is pushed into a long, narrow pipes, the push-in force is not transmitted to the head of the endoscope because of the buckling of the endoscope and friction around the endoscope, making long-distance inspection difficult [3]. Therefore, it is proposed that

The associate editor coordinating the review of this manuscript and approving it for publication was Jenny Mahoney.

a self-propelled mobile robot with an endoscopic function can be used for long-distance inspection in small-diameter pipes.

Self-propelled in-pipe mobile robots can be roughly classified into two types: wheeled robots driven by electricity [4]–[10] and wave propagation robots driven by air [11]–[15]. Wheeled robots move by rotating wheels with motors. The power source is placed outside the pipe because it is large, and the actuators are placed inside and outside the pipe. These robots are characterized by a fast electrical response and a relatively high robot movement speed. However, the following issues exist depending on the placement of the actuators. When the actuator is placed outside the pipe [10], the power transmission loss is large. In contrast, when the actuator is placed inside the pipe, a large and hard reduction gear cannot be carried inside the narrow pipe at high power and may get stuck in a complicated pipe layout. Therefore, it is difficult to adapt these robots to long-distance inspections [16] where large traction loads are applied.

Meanwhile, a wave propagation robot using air pressure moves by using the expansion and contraction of the actuator. Examples of wave propagation robots that have been developed are earthworm [11], [12], inchworm [9], [13], [14], and spiral tube [15] robots. Earthworm and inchworm robots are composed of a series of actuators that expand and contract by pressurizing and depressurizing air. By periodically expanding and contracting these actuators, the earthworm and inchworm robots move in a peristaltic motion [17], similar to real organisms. The spiral tube robot consists of a bundle of tubes that expand and contract according to the pressurization and decompression of air. The periodic expansion and contraction of these tubes causes a spiral motion [18], which moves the robot. Thus, most wave propagation robots are driven by the periodic pressurization and decompression of multiple actuators. The actuators of wave propagation robots are often small in size but highly flexible in terms of the force generated, despite their simple structure. Therefore, it is desirable to achieve long-distance inspection by generating a large traction force that corresponds to complex shapes in narrow pipes [19], [20]. However, the response of the actuator is slow owing to the compressibility of air [15]. In addition, the size of the solenoid valves commonly used for air control increases when the flow rate per hour increases. Thus, the controllable flow rate is limited in a small-diameter pipe, and the movement speed of the robot is small. In addition, the entire system is complicated because multiple air pressures are controlled by multiple electrical systems.

Therefore, research has been conducted to improve the response and simplify the system by focusing on the movement patterns of wave propagation robots [21]–[25]. These mechanisms realize periodic air pressurization and depressurization while reducing the size of the control system brought into the pipe and unifying the control and power systems with air. However, the flow rate that can be supplied is still small, and it is assumed that the response of the actuator is poor.

Therefore, we aim to develop a compact pneumatic valve that can realize periodic air pressure while maintaining a high flow rate, in response to the above issue. Existing pneumatic valves include globe valves and ball valves. A globe valve stops fluid by pressing against a plug in the middle of the flow path. There are various types of globe valves, such as needle valves with a needle-like tip and solenoid valves that use electromagnets to open and close the stopper. While these valves have the advantage of easy flow adjustment, they have difficulty in securing the flow rate. A ball valve opens and closes the flow path by rotating a spherical plug with a hole. This valve has low fluid resistance because the flow path is straight when the plug is fully open, but it has the problem of slow opening and closing speed of the valve [26].

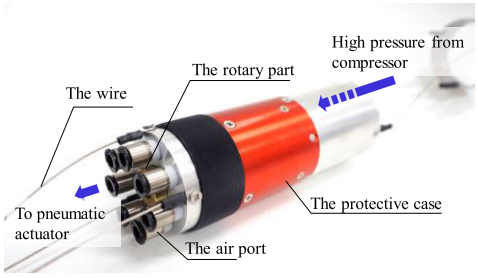

FIGURE 1. The overview of proposed valve.

In this study, we developed a new pneumatic valve (hereinafter ''CRV'') inspired by this ball valve, which has a large effective cross-sectional area of the flow path when fully open and uses a simple rotating mechanism to switch the flow path (Fig. 1). In addition, this valve was applied to a mobile robot developed by the authors as a wave propagation robot. This paper is organized as follows: Section II describes the position of the CRV to be developed in this study in comparison with related works. In Section III, the design concepts of the pneumatic valve and the in-pipe mobile robot are described. In Section IV, the prototype is introduced. In Section V, the modeling of the orifice of this pneumatic valve and its application to wave propagation robots is described. In Section VI, this pneumatic valve is applied to a wave propagation robot, and the driving experiment is described. The contributions of this study are as follows:

-We propose and develop a compact pneumatic valve that can realize periodic air pressure application while maintaining a high flow rate.

-Experiments have confirmed that the proposed mechanism can realize periodic air pressure switching with only one degree of freedom of rotational motion.

-The developed pneumatic valve was applied to a wave propagation robot, and the proper driving of the robot by the valve was confirmed.

-The effect of the pneumatic valve on the robot's motion is discussed based on theoretical and experimental results from the model, and the validity of the model is confirmed.

TABLE 1. Comparison of control mechanisms for long distance travel.

Drive method	Control mechanism	Location of the control mechanism	Responsiveness	The Flexibility of the moving mechanism	The lightness of the cable pulling load	Output Weight Ratio	Controllability and adaptability
Air	Proposed valve (Fig. 1)	Inside the pipe	HIGH	HIGH	HIGH	HIGH	HIGH
	Solenoid valve [9, 11-15]	Outside the pipe	LOW	HIGH	LOW	HIGH	VERY HIGH
	Mechanism [21-23]	Inside the pipe	MIDDLE	HIGH	HIGH	HIGH	VERY LOW
	Self-excited vibration valve [24, 25]	Inside the pipe	LOW	HIGH	HIGH	HIGH	LOW
	Solenoid valve [27, 28]	Inside the pipe	HIGH	HIGH	LOW	HIGH	VERY HIGH
Electricity	Motor [4-10]	Outside the pipe	HIGH	LOW	HIGH	LOW	VERY HIGH
		Inside the pipe	HIGH	LOW	HIGH	LOW	VERY HIGH

II. RELATED WORKS

The position of the CRV developed in this study will be compared to existing valves based on the systems used in related studies (Table 1). The discussion is divided into the following sections: Section A, where the pneumatic valve is placed outside the pipe and a pneumatic valve is required for each chamber; Section B, where the pneumatic valve is pulled inside the pipe and a pneumatic valve is required for each chamber; and Section C, where the pneumatic valve is pulled inside the pipe and supplies the chambers with a low degree of freedom.

A. PNEUMATIC VALVES ARE PLACED OUTSIDE THE PIPE AND EACH CHAMBER REQUIRES ITS OWN PNEUMATIC VALVE

This is the most widely used pneumatically driven system. It includes robots that mimic earthworms [11], [12], inchworms [9], [13], [14], and spiral tube robots [15]. Since a large pneumatic valve can be used outside the pipe, there is no restriction on the flow rate that can be supplied. The response delay can be improved by increasing the cross-sectional area of the air tube to increase the flow rate. However, as the distance traveled by the robot increases, the length of the air tube used to drive the robot needs to increase, and the air tube is also an air chamber, which causes a delay in response. In addition, because multiple tubes are arranged in parallel in the limited cross-sectional area of the tube, the increase in the cross-sectional area is limited, and a large traction is required. Furthermore, each time pressure is applied to the chamber, pressure is also applied to the pulling air tube, which is not energy efficient.

B. PNEUMATIC VALVES ARE PULLED INSIDE THE PIPE AND EACH CHAMBER REQUIRES ITS OWN PNEUMATIC VALVE

This is often used in pneumatically driven systems. In one example a pneumatic valve is connected to the tail of a robot using flexible linear cylinders [27], and in another an earthworm-type robot has pneumatic valves inside the robot [28]. The response delay can be reduced by pulling the pneumatic valve inside the pipe. In addition, a single air tube can be used to supply air from the pneumatic valve to the air pressure source located outside the pipe. However, with solenoid valves, which are commonly used to control air, the size of the solenoid valve increases when the flow rate per hour increases. This results in a large load during traction. Therefore, there is a trade-off between the flow rate and the load during traction. In addition, the number of pneumatic valves must be the same as the number of chambers to be pulled, which increases the weight. The pneumatic valves themselves are rigid, which impairs flexibility, and solenoids are used to drive the solenoid valves, which require several watts of power and pose a risk of ignition when inspecting the pipe for flammable fluids.

C. PNEUMATIC VALVE PULLED IN THE PIPE TO SUPPLY THE CHAMBER WITH LOW DEGREE OF FREEDOM

This is a new pneumatically driven system that is beginning to be used. There is (i) a mechanism with different orifice holes in the air tube [21], (ii) a mechanism that uses springs and dampers to generate periodic motion [22], and (iii) a mechanism that allows forward and backward motion with mechanically fewer air tubes [23]. We consider that (i) has the disadvantage of not being able to switch between forward and backward motion, and (ii) has poor controllability because of the slow moving speed and the inability to stop. In (iii), there are two large air tubes. In addition, (i)–(iii) cannot be separated as pneumatic valves and are designed for exclusive use, which limits the range of applications. Furthermore, they are not easy to repair in cases of failure. Therefore, we focused on the mechanism for separating the pneumatic valves.

To isolate the air valve, a valve that realizes periodic pressurization and depressurization of air using self- excited

oscillation by a small magnet [24], and a simple valve that realizes pressurization and depressurization of air by controlling the air pressure [25] have been developed. These valves realize periodic pressurization and depressurization of air while reducing the size of the control system to be brought into the pipe and unifying the control and power systems with air. In addition, they have a simple structure and operate only by supplying air through a single air tube, which simplifies the mechanism and reduces the risk of failure. However, the flow rate that can be supplied is small, and it is difficult to adapt to robots that require a high flow rate. Furthermore, the robot cannot switch between the forward and backward motions. In addition, the input pressure must be changed to determine the traveling speed as desired, and it is not easy to change the speed and input pressure independently. Therefore, the controllability of the system is poor, and the range of adaptation is narrow.

III. DESIGN AND CONCEPT

This section describes the design concept of the CRV to be developed and the wave propagation robot to which the CRV will be applied.

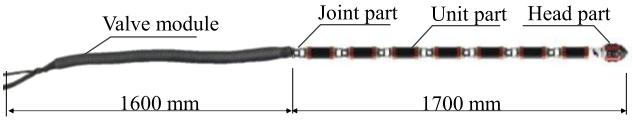

FIGURE 2. The schematic of proposed mechanism internal structure.

A. DESCRIPTION OF THE IN-PIPE MOBILE ROBOT (PEW-RO V)

As a wave propagation robot, the authors have developed a mobile in-pipe robot (hereinafter "PEW-RO V") (Fig. 2). The PEW-RO V is designed for continuous inspection of a 100 A pipe (inner diameter: 108 mm), which is one of the smallest pipes, for approximately 100 m [29]–[32]. The PEW-RO V mimics the peristaltic motion of an earthworm, which is characterized by a small amount of space required for movement and has a large footprint that presses against the pipe during movement, resulting in a large traction force. The maximum travel speed of the PEW-RO V is 50 mm/s, and the maximum traction force is 300 N. The traveling performance of the system has been confirmed through field experiments, and it is expected to be used as an inspection device in the future [33].

The PEW-RO V consists of a head part, unit parts, joint parts, pneumatic components (valves, compressors, and regulators), a microcomputer, a power supply for the microcomputer, and a power supply for the valves. The unit parts use axial fiber-reinforced pneumatic artificial muscles (hereafter artificial muscles) [34], [35]. The unit part expands in the radial direction and contracts in the axial direction when air pressure is applied. When multiple units are connected and pneumatic pressure is applied in turn, they move in a peristaltic motion, as shown in Fig. 3, to propel the pipe. All artificial muscles in this robot are 100 mm long. The artificial muscles used as unit parts are highly resistant to the conditions of the pipe and can run in a real environment without changing the running mode during operation [32]. A direct-acting solenoid valve was used to control the air pressure of the PEW-RO V.

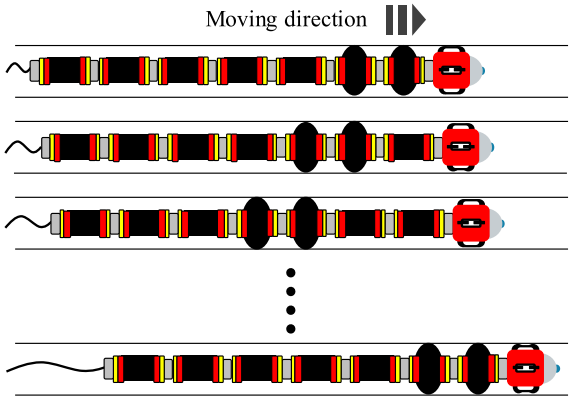

FIGURE 3. The schematic of peristaltic motion robot in pipe.

B. DESIGN AND CONCEPT OF PROPOSED VALVE

Wave propagation robots often move by periodically driving the pneumatic actuators. In these robots, multiple pneumatic actuators are connected to each other and periodically driven by connected pneumatic valves. Therefore, although structurally the robot has multiple inputs, it can be regarded as having a single degree of freedom in its motion because it can only perform a constant repetitive motion.

Thus, the authors thought that it would be possible to drive pneumatic actuators with a compact structure by rotating the channels and switching which channels are connected to each pneumatic actuator.

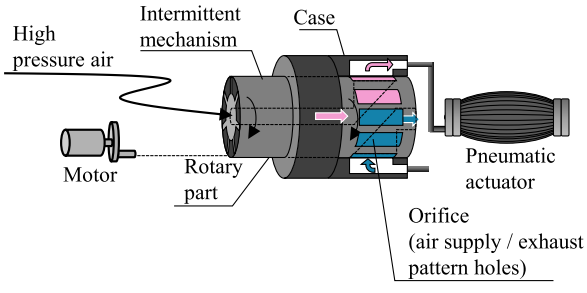

FIGURE 4. The schematic of the CRV internal structure.

Fig. 4 shows a schematic diagram of the internal structure of the proposed CRV, and Fig. 5 shows a schematic diagram of both the pneumatic valve and robot drive. This valve consists of a rotary part with a flow path, a motor for driving the rotary part, a protective case, and an intermittent mechanism. In the rotary part, air supply holes, which supply air pressure from the air pressure source to the pneumatic actuator, and

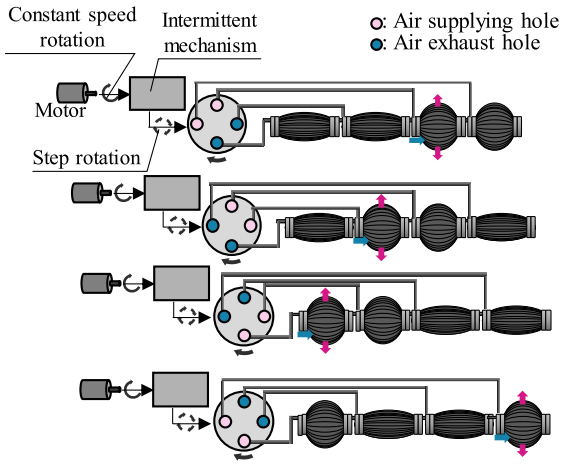

FIGURE 5. The appearance of a robot moving motion and the CRV.

exhaust holes, which release the pressure from the pneumatic actuator, are regularly arranged in the same circumferential direction. When the rotary part is rotated by a motor, the pneumatic actuators are connected to the supply and exhaust holes on the rotary part in order. Therefore, the periodic drive is realized by the arrangement of the air supply and exhaust holes. We assume that the CRV can realize periodic air pressure even in a small sized pipe, and that the system of a wave propagation robot with periodic drive can be miniaturized and consolidated. In addition, the opening and closing of the orifice by rotation does not interfere with the flow path when fully open, as in the case of a ball valve. This ensures a high flow rate. The flow path is opened and closed by the holes located on the sides of the rotary part and holes on the inside of the protective case. Thus, there is no need to reduce the load on the rotary part due to high pressure, and there is no need for a special seal to prevent air leakage. In addition, because the step opening and closing is realized by an intermittent mechanism installed in the rotary part, high pressure air with a high flow rate can be controlled without using a controller.

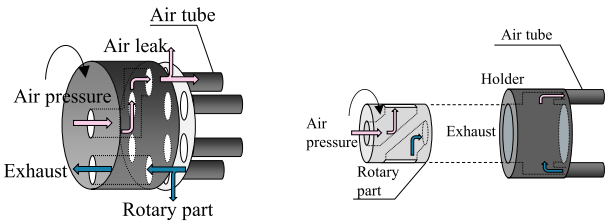

(a) The schematic of trust air flow mechanism.

(b) The schematic of radial air flow mechanism.

FIGURE 6. The schematic of Pneumatic distribution method.

C. AIR PRESSURE DISTRIBUTION SYSTEM FOR THE CRV

Fig. 6(a) shows a schematic diagram of the thrust distribution system, and Fig. 6(b) shows a schematic diagram of the radial distribution system. In the thrust distribution system, the orifices are located on the plane perpendicular to the rotation axis. Although the structure is simple, the sliding surface is subjected to the force of high-pressure air from one direction during high-pressure, high-flow driving, which causes gaps and air leaks, and the mechanism to prevent air leaks is large. On the other hand, the radial distribution method has orifices on the sides of the rotating parts, and supplies and exhausts air in the circumferential direction. The radial distribution system is more costly than the thrust system because of the high-precision fit, but because the shaft is inserted in the bearing, there is no risk of air leakage and the mechanism itself can be simplified. Compared with the thrust system, the radial system has a larger flow path cross-section and allows for a higher flow rate. In the thrust system, air leakage occurs at the sliding surface; therefore, it is necessary to prevent air leakage or reduce the cross-sectional area of the flow path to limit the flow rate through the orifice. The radial system, however, not only prevents air leaks by fitting the shaft directly into the bearing, but also makes it possible to increase the cross-sectional area of the flow path.

Considering the above points, the radial system was adopted for the CRV.

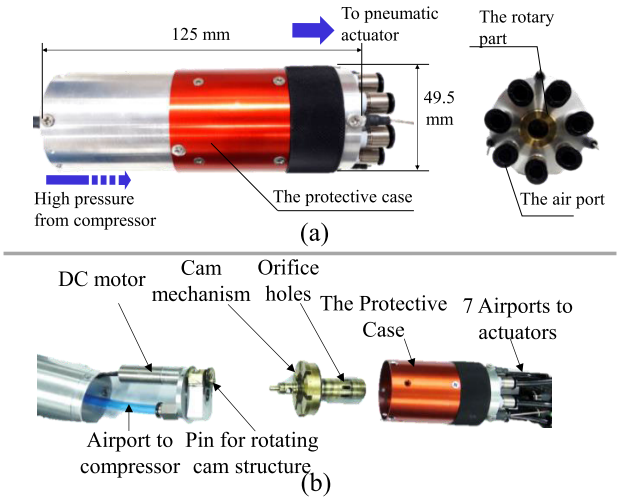

FIGURE 7. (a)The detailed size of proposed valve. (b) The exploded view of the proposed valve.

IV. DEVELOPMENT

In this section, we describe the prototype that we fabricated based on the design considerations discussed in the previous section. The developed CRV is illustrated in Fig. 7. It has a length of 125 mm and mass of 800 g. The CRV consists of a port for the air tube to connect to the compressor, a DC motor, a rotary part with cam grooves and orifices, a pin that transmits the rotation of the DC motor to the rotary part, a protective case, and seven ports for the air tube to connect to the pneumatic actuator. In addition, an umbilical cable, which consists of a high-pressure air supply tube and a motor power supply cable, is connected to the rear of the CRV. In addition, suspension wires are attached to the front and

TABLE 2. The specification of DC motor.

Values at nominal voltage	Quantity
Nominal voltage	24 V
No load speed	12800 rpm
No load current	25.5 mA
Nominal speed	10600 rpm
Nominal torque (max. continuous torque)	11.2 mNm
Nominal current (max. continuous torque)	0.652 A
Stall torque	68.5 mNm
Stall current	3.86 A
Max. efficiency	84%

TABLE 3. The specification of Gearhead.

Gearhead data	Quantity
Reduction	16:1
Absolute reduction	5625/361
Number of stages	2
Max. continuous torque	0.25 Nm
Max. intermittent torque	0.35 Nm
Max.efficiency	80%
Average backlash no load	1.2 °
Gearhead length	20.8 mm
Max.transmittable power (continuous)	3.2 W
Max.transmittable power (intermittent)	4 W

rear of the CRV, with the front wires connected to the robot body and the rear wires connected to the umbilical cable. This structure prevents direct tension from being applied to the internal structure of the robot or motor of the CRV.

The DC motor used in this study was a Maxon DCX16L (with graphite brushes and ball bearings). The gear reducer is a Maxon GPX16 (with a built-in Hall sensor), and a two-stage gear ratio of 16:1 was used. Table 2 lists the specifications of the DC motor, and Table 3 lists the specifications of the reduction gear. The protective case was made of JIS H 4040 A5056B material with an anodized finish. The rotary part was made of JIS H 3250 C3604B material. The orifices are rectangular, 3.0 mm wide and 8.5 mm long. In this study, this material was used as an initial study.

Table 4 lists the specifications of the PEW-RO V equipped with the fabricated CRV. Table 4 also lists the specifications of the PEW-RO V equipped with the solenoid valve for comparison. The total length and weight of the PEW-RO V with the CRV were 45 % and 43 % of those of the PEW-RO V with a solenoid valve, respectively.

Although the valve fabricated in this paper was designed for a specific environment, the findings obtained in this study are useful because they can be applied to a variety of environments.

TABLE 4. The comparison of specifications when the CRV and solenoid valve module are mounted on this robot.

	Robot equipped with solenoid valve	Robot equipped with CRV	Ratio of CRV and solenoid valves
Length [m]	3.3	1.8	0.45 [%]
Weight [kg]	11	6.3	0.43 [%]

V. MODELING

In this section, we describe the modeling of the proposed CRV and its application to a wave propagation robot. We consider a system consisting of a CRV and a wave propagation robot. Because the wave propagation robot is operated by air pressure, a compressor is used as the air pressure source. The air supplied from the compressor passes through the CRV to flow into the actuator of the wave propagation robot. The actuator of the wave propagation robot continuously changes its shape owing to the inflow of air, so the volume of air in the actuator is constantly changing. Therefore, to track this behavior, it is necessary to understand the changes in the orifice area of the CRV. This makes it possible to theoretically calculate the traveling speed of the wave propagation robot when using the CRV.

In Section A, we model the change in the orifice area of the CRV, and in Section B, we describe the shape change model of the actuator of the wave propagation robot and explain the theoretical running speed of the robot when the CRV is applied to the wave propagation robot.

A. MODELING OF ORIFICE HOLE OPENING/CLOSING MECHANISM

This section describes the opening and closing mechanisms of the orifices. It is desirable to open and close the orifice intermittently. In this study, a mechanism for intermittent rotation was adopted using a DC motor with constant rotation. There are other methods for controlling the motor angle to achieve an intermittent motion. However, because these methods require the installation of sensors and other equipment, the possibility of failure increases when considering its use in a real environment. In addition, we thought that the intermittent opening and closing of the CRV should be done without using a sensor and using a DC motor to account for the environmental resistance and the robustness needed for use in a real environment. Thus, we thought it would be better to use a mechanism to realize step opening/closing, because it does not require feedback using a sensor and can be driven by simple voltage application.

Table 5 summarizes the parameters used in the model. Fig. 8 shows the schematic diagram of the intermittent mechanism and the rotation transmission used in this study, and Fig. 9 shows the rotation of the intermittent mechanism and the motor.

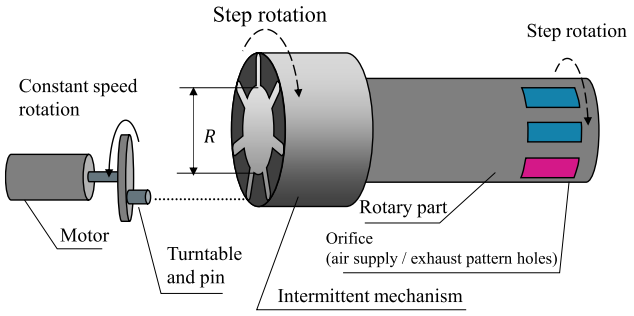

FIGURE 8. The structure of intermittent mechanism and motor.

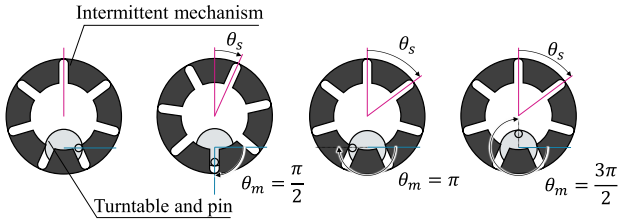

FIGURE 9. The appearance of intermittent mechanism rotation.

TABLE 5. The parameter of modeling the compact rotary valve.

Symbol	Definition
θ_{m} [rad]	Rotation angle of input side rotating component drive motor
ω_{m} [rad/s]	Angular velocity of input side rotating component drive motor
r_{m} [m]	Rotating diameter of the rotating pin of the motor for driving the input side rotating parts that meshes with the cam groove
θ_{s} [rad]	Output side rotating parts rotation angle
n [-]	An integer greater than or equal to 0
k [-]	Number of teeth on cam
$x(t)$ [m]	Moving displacement of rotating parts
a [m]	The width of orifice hole
b [m]	The length of orifice hole
θ_{a} [rad]	The angle corresponding to the width of the orifice hole

The rotation angle of the motor on the input side is θ_m, and the rotation angle of the rotary part on the output side is θ_s. The rotary part on the output side exhibits two different behaviors during one rotation of the motor on the input side. For an integer n greater than or equal to 0, when $2n\pi < \theta_m < (2n+1)\pi$, the cam structures of the input motor and the output rotary part mesh, and the rotary part rotates θ_s. When $(2n+1)\pi < \theta_m < 2(n+1)\pi$, the cam structures of the input motor and output rotating parts do not mesh, and only the input motor rotates idle. By repeating this process, intermittent rotary motion was realized.

Next, the behavior of the rotary part by intermittent rotary motion is described. For simplicity, the cam structure of the rotary part is approximated as a straight part instead of a circular part. Therefore, the rotation of the input motor causes a rotational motion of the rotary part, but by approximation, the rotary part is considered to move in a straight line. If the rotation angle and angular velocity of the input motor are θ_m and ω_m respectively, these can be expressed as (1) using the time variable t.

$$\theta_{\mathrm{m}} = \omega_{\mathrm{m}} t \tag{1}$$

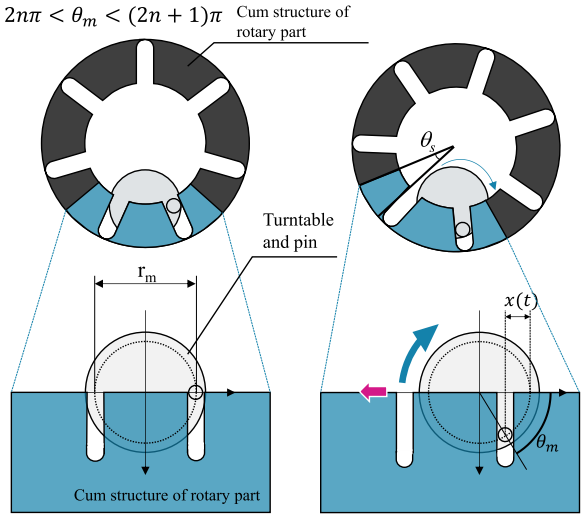

FIGURE 10. The appearance of intermittent mechanism.

The rotating diameter of the rotating pin of the input side motor that meshes with the cam groove is r_{m}, and the rotation of the input side motor by θ_m is shown in Fig. 10. The diameter of the cam grooves is R, and the number of cam grooves is k. These can be expressed as (2).

$$R\pi \cong k r_{\mathrm{m}} \tag{2}$$

Under $2n\pi < \theta_m < (2n+1)\pi$, the displacement $x(t)$ of the rotating part is expressed by (3).

$$x(t) = \begin{cases} \dfrac{r_{\mathrm{m}}}{2}(2n+1-\cos\theta_{\mathrm{m}}), & 2n\pi < \theta_{\mathrm{m}} < (2n+1)\pi \\ (n+1)r_{\mathrm{m}}, & (2n+1)\pi < \theta_{\mathrm{m}} < 2(n+1)\pi \end{cases} \tag{3}$$

The relationship between $x(t)$ and $\theta_{\mathrm{s}}(t)$ can be expressed by (4).

$$\theta_{\mathrm{s}}(t) = \frac{2x(t)}{R} \tag{4}$$

From (3) and (4), the relationship between θ_{m} and θ_{s} can be expressed as shown in Fig. 11(a).

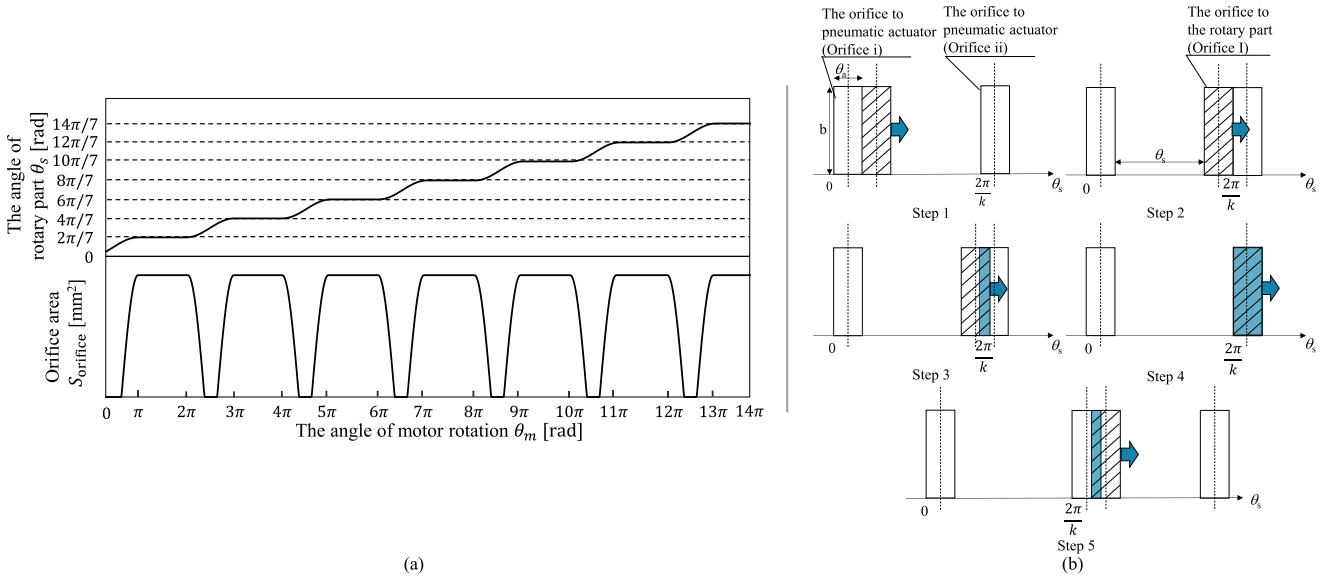

FIGURE 11. (a) The relationship between the angle of motor rotation and the angle of rotary part, orifice area. (b) The moving appearance of orifice.

Next, we considered the opening and closing behavior of the orifices. Fig. 11(b) shows a schematic diagram of the behavior of the orifices opened in the rotary part, and the orifices opened in the protective case. In this study, we focus on two orifices opened consecutively in the protective case (hereinafter "orifice i" and "orifice ii") and one orifice with a rotary part (hereafter "orifice I"). The orifices are rectangular in shape with a width a [mm] and length b [mm]. The angle of the rotary part corresponding to the width a [mm] of the orifice is defined as θ_a. Air flows at the overlap of these orifices. STEP 1 in Fig. 11(b) shows the moment when orifice i and orifice I finish overlapping and become blocked. This moment is defined as time $t = 0$. Next, STEP 2 in Fig. 11(b) shows the moment when orifice I moves because of the rotation of the rotary part and begins to overlap with orifice ii. During the transition from STEP 1 to STEP 2, the area of orifice ii is zero because the orifice is in the closed state (5).

$$S_{\text{orifice}} = 0, \quad 0 \leq \theta_s(t) \leq \frac{2\pi}{k} - 2\theta_a \tag{5}$$

Next, STEP 3 in Fig. 11(b) shows the overlap between orifice ii and orifice I. Furthermore, STEP 4 in Fig. 11(b) shows the moment when orifices ii and I completely overlap. Therefore, in the transition from STEP 2 to STEP 4, the orifices changed from a closed state to an open state. The area of orifice ii at that time is given by (6).

$$S_{\text{orifice}} = \frac{Rb}{2}\left(\theta_S(t) + 2\theta_a - \frac{2\pi}{k}\right), \frac{2\pi}{k} - 2\theta_a \leq \theta_s(t) \leq \frac{2\pi}{k} - \theta_a \tag{6}$$

Finally, STEP 5 in Fig. 11(b) shows the state in which orifice I is moving. Therefore, in the transition from STEP 4 to STEP 5, the orifice changed from an open state to a closed state. The area of orifice ii at this time is given by (7).

$$S_{\text{orifice}} = \frac{Rb}{2}\left(\frac{2\pi}{k} - \theta_s(t)\right), \frac{2\pi}{k} - \theta_a \leq \theta_s(t) \leq \frac{2\pi}{k} \tag{7}$$

B. SHAPE CHANGE MODEL OF PNEUMATIC ACTUATOR FOR WAVE PROPAGATION ROBOT

1) APPLICATION OF A MECHANICAL EQUILIBRIUM MODEL FOR ARTIFICIAL MUSCLES

The CRV developed in this study can change the driving cycle of the PEW-RO V by changing the rotation speed with the voltage applied to the motor. However, because the area of the orifice changes by changing the rotation speed, the volume flow rate of the air applied to the artificial muscle changes, and the contraction amount of the artificial muscle also changes. Therefore, when the CRV is used to drive the PEW-RO V equipped with artificial muscles, the driving performance of the PEW-RO V can be fully demonstrated by determining the most appropriate rotation speed and applied pressure. Thus, the purpose of this section is to determine the relationship between the rotation speed and the applied pressure by modeling the running speed of the PEW-RO V with artificial muscles and CRV. To model the running speed of the robot according to the rotation speed and the applied pressure of the CRV, the dynamic characteristics of the artificial muscles are necessary, but the dynamic characteristics are very complicated because the artificial muscles are pneumatically driven. Therefore, we focused on a mechanical equilibrium model that deals with the static characteristics of artificial muscles. In this model, the shape of the artificial muscle is obtained by determining the internal pressure and load of the artificial muscle, and the amount of contraction in the equilibrium state was determined. First,

TABLE 6. The parameters used in the mathematical of artificial muscle.

Symbol	Definition	Value
P [MPa]	Internal air pressure of artificial muscle	
F [N]	Load	
x_d' [mm]	Desirable contraction	
G_1, G_2, G_3 [-]	Constants that determine the force	
α [-]	Approxomation constant number	1.4
l_0 [mm]	Length of artificial muscle	100
K [Pa]	Elastic modulus of rubber	7.7×10^6
t [mm]	Thickness of artificial muscle	1
M [-]	Fiber constant number	1
n [-]	Number of fiber	
b [mm]	Width of fiber	

we explain the mechanical equilibrium model of artificial muscles. The validity of this model was confirmed in a previous study [34]. The shape of the artificial muscle is shown in Fig. 12, and its parameters are listed in Table 6.

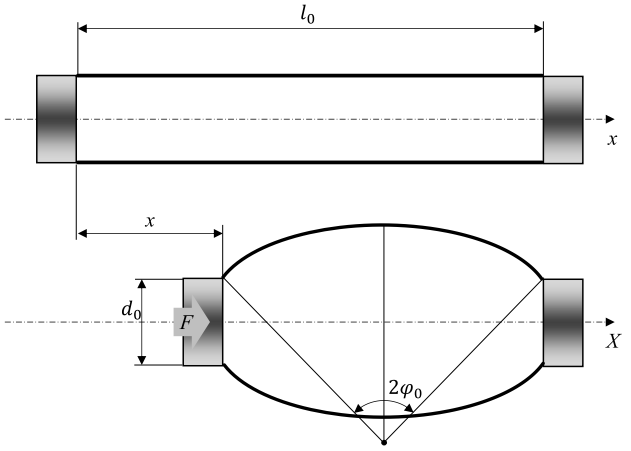

FIGURE 12. The geometric model of artificial muscle.

When the shape of the artificial muscle is modeled as shown in Fig. 12, the relationship between the contraction volume x, load F, and pressure P of the model is shown in (8). Each function in (8) is given by (9)–(12). The theoretical and experimental values of the mechanical equilibrium model for artificial muscles with a diameter of 56 mm and length of 100 mm installed in the robot are shown in Fig. 13. The vertical axis represents the amount of contraction, and the horizontal axis represents the equilibrium pressure. For simplicity, no load was assumed in the mechanical equilibrium model, and no load was applied in the experiments. Fig. 13 shows that the mechanical equilibrium model adequately reproduces the characteristics of the artificial muscles installed in the robot, confirming the usefulness of the model.

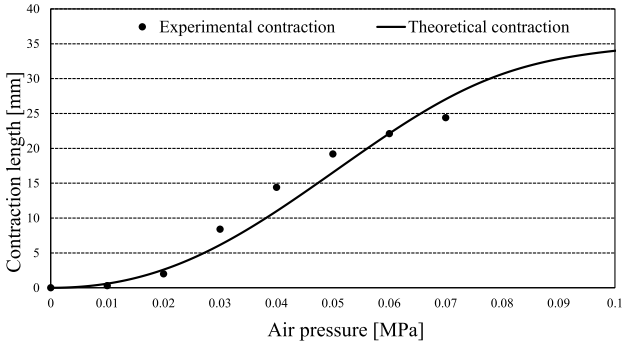

FIGURE 13. The results of relationship between air pressure and theoretical/experimental contraction length.

This model was used to obtain the running model of the PEW-RO V equipped with a CRV.

$$P(\varphi_0, F) = \frac{FG_2(\varphi_0) + G_1(\varphi_0)}{G_3(\varphi_0)} \tag{8}$$

$$\varphi_0 = \frac{2\alpha l_0^{1.5} x}{(l_0 - x)^2 + \alpha^2 x l_0} \tag{9}$$

$$G_1(\varphi_0) = \frac{4Kt}{d_0}\left[\frac{l_0}{d_0}\right]^2\left[\frac{\sin(\varphi_0) - \varphi_0\cos(\varphi_0)}{\varphi_0^2}\right] \tag{10}$$

$$G_2(\varphi_0) = \frac{M\tan\varphi_0}{d_0 nb} \tag{11}$$

$$G_3(\varphi_0) = 2\left[\frac{l_0}{d_0}\right]^2\left[\frac{\sin(\varphi_0) - \varphi_0\cos(\varphi_0)}{\varphi_0^2}\right] + 4\frac{l_0}{d_0}\frac{\sin\varphi_0}{\varphi_0} - \frac{\pi d_0 M}{4nb}\tan\varphi_0 \tag{12}$$

2) CONSTRUCTION OF A PNEUMATIC VALVE MODEL BY APPLYING THE MECHANICAL EQUILIBRIUM MODEL OF ARTIFICIAL MUSCLES

By applying the mechanical equilibrium model of the artificial muscles described in the previous section, we consider the model for the proposed CRV. In the CRV model, the motor speed changes with the voltage applied to the motor, and the area of the orifices changes with the rotation speed. Two out of seven ports on the rotary part of the CRV are designed as air supply holes, and five ports are designed as exhaust holes. Because the area of the orifices is rectangular (ab [mm^2]), as described in the previous section, the opening and closing behaviors are shown in Fig. 14. The positive area represents the air supply, and the negative area represents the exhaust. air supply holes, and five ports are designed as exhaust holes.

Next, we consider the time variation of the orifices of the CRV and the dynamic application of the mechanical equilibrium model.

First, we considered the air supply. During the air supply, the compressor is the primary pressure (constant pressure), and the pressure inside the artificial muscle is the secondary pressure. The airflow rate depends on the area of the orifice holes and the differential pressure between the primary and secondary pressures, which vary from time to time in the

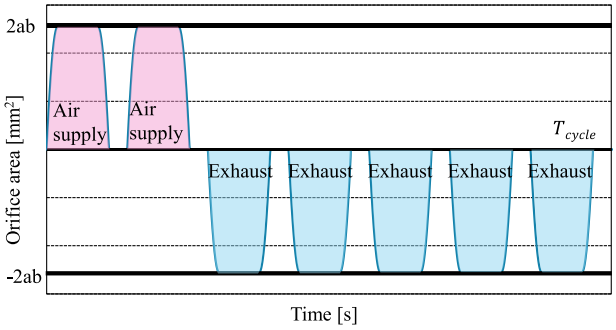

FIGURE 14. The opening and closing behavior of air supplying and exhaust orifice of proposed mechanism.

TABLE 7. The parameters of (14) and (15).

Symbol	Definition
Q_t [L/min]	Volume flow rate
C [-]	Flow coefficient
S_t [m^2]	Orifice area
P [Pa]	Primary pressure (supply puressure by compressor)
P_t [Pa]	Secondary pressure (internal prussure of artificial muscle)
ρ [kg/m^3]	Air density

case of the CRV. We consider a time $T = t$ [s] and a time $T = t+\Delta t$ [s] after a small period of time (Δt [s]). Assuming that the pressure inside the artificial muscle at time $T = t$ is P_t and the area of the orifice is S_t, the flow rate at that moment can be obtained from (13).

$$Q_t = CS_t\sqrt{\frac{2\,(P - P_t)}{\rho}} \tag{13}$$

This gives the volume ΔV of air flowing into the artificial muscle within a small time period from time $T = t$ by (14).

$$\Delta V = Q_t \Delta t \tag{14}$$

The parameters in the equation are listed in Table 7. This inflow of air causes the artificial muscle to contract from x_t to $x_{t+\Delta t}$ while changing its shape based on the mechanical equilibrium model, and the internal pressure increases from P_t to $P_{t+\Delta t}$. By repeating this process, we thought that we could handle the dynamic contraction behavior of the artificial muscle using the mechanical equilibrium model.

Next, we considered the exhaust of the artificial muscle. During exhaustion, the pressure inside the artificial muscle becomes the primary pressure, and the secondary pressure becomes the atmospheric pressure (constant pressure). This change also considers the dynamic application of the mechanical equilibrium model of the artificial muscle and considers the change in the small time period Δt. If the pressure inside the artificial muscle at time $T = t$ is P, the atmospheric pressure is P_t, and the area of the orifice is S_t, the flow rate at that moment can be obtained from (14),

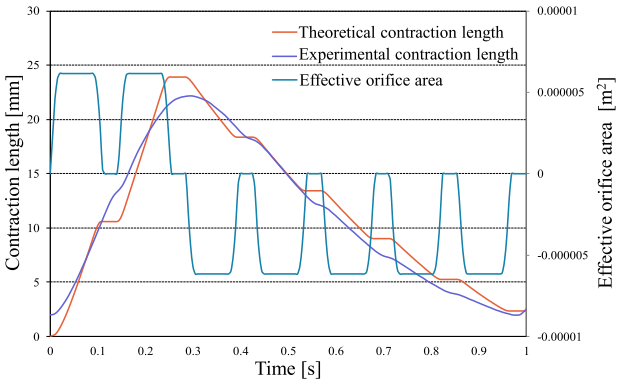

FIGURE 15. The relationship between theoretical contraction length and experimental contraction length in 60 rpm, 0.4 MPa.

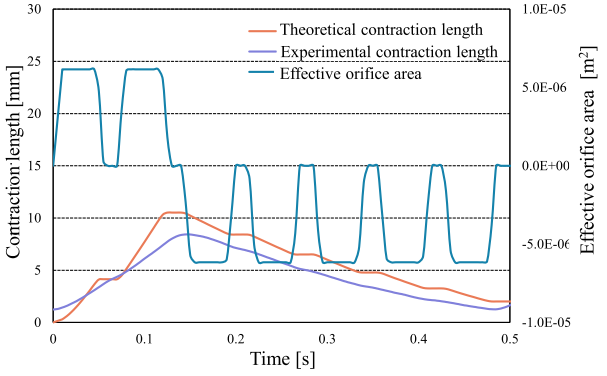

FIGURE 16. The relationship between theoretical contraction length and experimental contraction length in 120 rpm, 0.4 MPa.

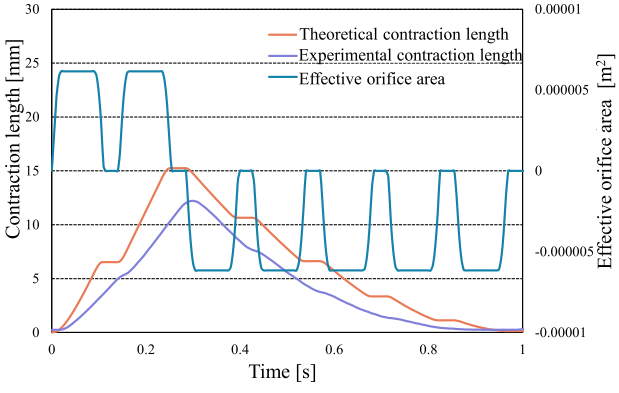

FIGURE 17. The relationship between theoretical contraction length and experimental contraction length in 60 rpm, 0.2 MPa.

paying attention to the primary and secondary pressures as in the air supply. This outflowing air causes the artificial muscle to elongate from x_t to $x_{t+\Delta t}$ while changing its shape based on the mechanical equilibrium model, and the internal pressure decreases from P_t to $P_{t+\Delta t}$. With the previous section in mind, Fig. 15, 16, and 17 show the theoretical contraction and expansion behavior of the artificial muscles and the measured experimental contraction and expansion behavior

of the artificial muscles when the CRV was driven at different rotational speeds and different applied pressures. In Fig. 15, the CRV was driven at a rotation speed of 60 rpm and an applied pressure of 0.4 MPa; in Fig. 16, the CRV was driven at a rotation speed of 120 rpm and an applied pressure of 0.4 MPa; in Fig. 17, the CRV was driven at a rotation speed of 60 rpm and an applied pressure of 0.2 MPa. The left vertical axis of the graphs shows the amount of contraction of the artificial muscle, and the right vertical axis shows the area of the air supply and exhaust orifice holes.

From these results, it can be concluded that the model adequately reproduces the contraction and elongation characteristics of the artificial muscle induced by CRV.

3) DEVELOPMENT OF A MODEL FOR CALCULATING VELOCITY WITH CRV BY APPLYING A MECHANICAL EQUILIBRIUM MODEL OF ARTIFICIAL MUSCLE

In this section, we construct a theoretical velocity model of PEW-RO V using CRV with a mechanical equilibrium model of artificial muscles. The contraction and extension of the artificial muscles during the supply-discharge transition were clarified by the theoretical supply-discharge model with CRV, which applied the mechanical equilibrium model described in the previous section. Therefore, we determined the running speed of the PEW-RO V by considering the movement of the artificial muscles during the transition. It was assumed that each unit was driven in an ideal state, where the supply and exhaust were instantaneous. However, in actual driving, there are some units that supply air, and some are exhausting air.

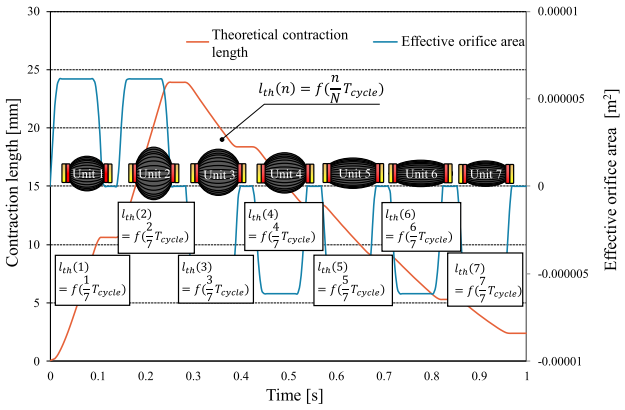

FIGURE 18. The relationship between contraction length and each unit part of peristaltic crawling robot.

The transition states of each unit of the PEW-RO V with CRV from the mechanical equilibrium model of the artificial muscles are shown in Fig. 18. The running speed was calculated by considering the state of each unit.

If the contraction l_{th} of the artificial muscle calculated by the mechanical equilibrium model of the artificial muscle is (15) using the time variable t, the contraction-extension transition state of the artificial muscle in the nth unit is expressed as (16). The parameters in the equation are listed in Table 8.

TABLE 8. The parameters of (15), (16), and (17).

Symbol	Definition
N [-]	Total number of pneumatic actuator
T_{cycle} [s]	The cycle of time
l_{th} [mm]	The theoretical contraction amount of the unit
l_{max} [mm]	The maximum length of the contraction amount of the unit
l_{loss} [mm]	The loss length by pressurization
v_{th} [mm/s]	The theoretical speed of the robot

$$l_{th} = f(t) \tag{15}$$

$$l_{th}(n) = f\left(\frac{n}{N}T_{cycle}\right) \tag{16}$$

The subscripts correspond to each unit number, the total number of units is N, and the cycle time is T_{cycle}. The artificial muscles mounted on the robot had both contraction and extension motions. If we focus on the first part of the robot, the unit part before the grasping unit contracts, and the unit part after the grasping unit extends. The contraction motion acts as a negative component of the velocity, whereas the extension motion acts as a positive component. Assuming that the maximum contraction is l_{max}, the pressurized length is l_{loss}, and the jth unit part is the grasping unit, the traveling speed v_{th} of the robot is expressed as (17).

$$v_{\text{th}} = \frac{-\sum_{k=1}^{j-1} l_{\text{th}}(k) + \sum_{k=j+1}^{N} \{(l_{\text{max}} - l_{\text{loss}}) - l_{\text{th}}(k)\}}{T_{\text{cycle}}} \tag{17}$$

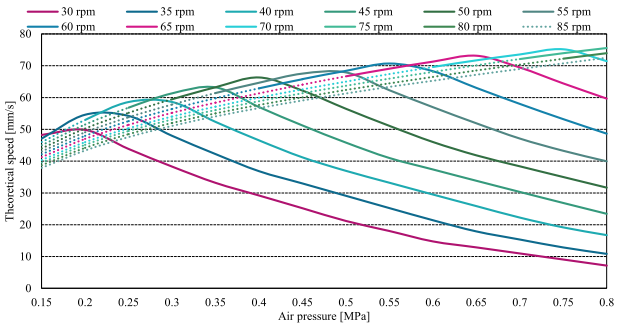

FIGURE 19. The theoretical speed at each applied pressure and rotation speed of peristaltic crawling robot. The dotted line in the graph is the area where the PEW-RO V cannot travel.

Using this equation, the running speed of the PEW-RO V is calculated. The theoretical running speeds for each pressure and rotation speed are shown in Fig. 19. The vertical axis shows the traveling speed, and the horizontal axis shows the applied pressure. The dotted line in the graph is the area where the PEW-RO V cannot travel because the unit of the PEW-RO V does not contract sufficiently to grasp the pipe wall. At each rotation speed, the traveling speed is reduced at low pressure due to insufficient contraction and at high pressure due to insufficient exhaust.

VI. EXPERIMENT

In this section, it is confirmed that the PEW-RO V equipped with the proposed CRV can be propelled in the pipe. The validity of the model developed in Section V is discussed based on the experimental results.

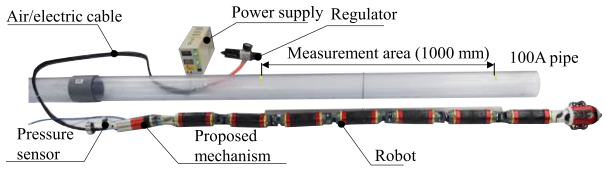

FIGURE 20. The experimental setup of the experiments to confirm driving robot.

A. DRIVE EXPERIMENT

A schematic of the experimental environment is shown in Fig. 20. The CRV is connected to the tail of the PEW-RO V. A high-pressure air supply tube and a power supply cable to the motor must be connected to the CRV. The CRV is driven at a speed that completes one cycle in one second, which is easy to check. The applied pressure was adjusted by visually checking the expansion diameter of the artificial muscles of the robot to increase the pressure to a level at which all the artificial muscles could grasp the pipe. The running pipe was a transparent 100A pipe (inner diameter: 108 mm) with a length of 3 m. The inside of the pipe is observed. The umbilical cable was 3 m in length. A bird's eye view was taken the traveling of the robot.

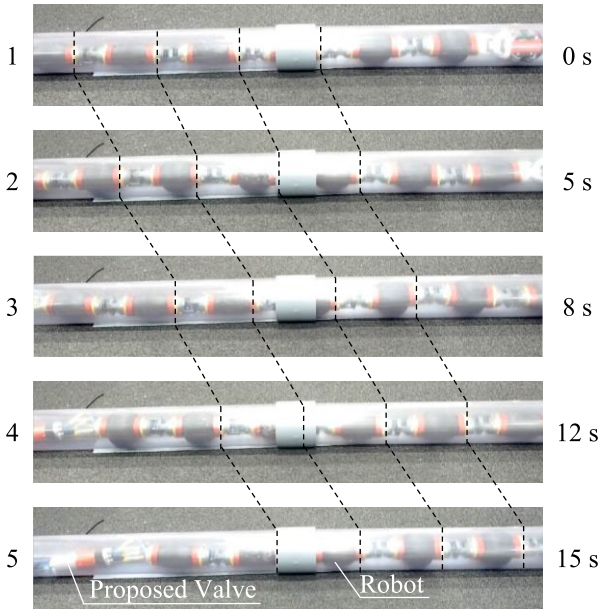

FIGURE 21. The driving appearance with proposed valve.

Fig. 21 shows the running of the PEW-RO V equipped with the CRV. In this experiment, we confirmed that the proposed CRV can reproduce peristaltic motion and propel the robot in the pipe.

B. MODEL VERIFICATION DRIVING EXPERIMENT

The purpose of this experiment is to verify the validity of the constructed model. In a previous study, the speed of the PEW-RO V was calculated only by the amount of contraction of the artificial muscle and the time required for one cycle; in this study, we developed a model for calculating the running speed that takes into account the contraction and elongation process by applying the mechanical equilibrium model of the artificial muscle in addition to the applied pressure and rotation speed of the CRV. Thus, it is necessary to confirm the validity of this model.

The CRV is connected to the tail of the PEW-RO V, and an umbilical cable was connected. The applied voltage and pressure corresponding to each rotation speed were applied to the CRV to drive the PEW-RO V. The traveling pipe was a 100A pipe (inner diameter: 108 mm), which was transparent so that the inside could be observed.

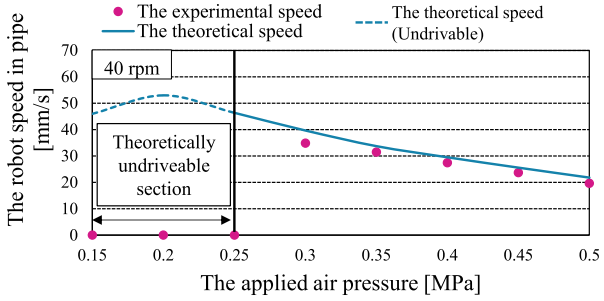

FIGURE 22. The relationship between robot speed and applied air pressure in 40 rpm. The dotted line indicates that the robot cannot run.

Fig. 22 shows the theoretical values calculated by the model and the experimental values measured by the experiment for the traveling speed of PEW-RO V in the pipe for each applied pressure when the CRV is rotated at 40 rpm. The vertical axis shows the traveling speed of the PEW-RO V, and the horizontal axis shows the applied pressure. At this speed, the theoretical and experimental values agreed for all applied pressures except 0.25 MPa. This is due to the fact that the supply and exhaust holes overlapped for a sufficient time due to the low rotation speed. At the applied pressures of 0.15 MPa and 0.2 MPa, the model calculated that grasping in the pipe was not possible due to insufficient shrinkage, and the machine could not run. However, in the running experiment, it was confirmed that the machine did not run even at 0.25 MPa. This is because the applied pressure was small, the flow resistance was affected, and the CRV did not contract to the amount calculated by the model in actual driving. Fig. 23 shows the theoretical values calculated from the model and the experimental values measured for each applied pressure when the CRV was rotated at 60 rpm. The vertical axis shows the traveling speed of the robot, and the horizontal axis shows the applied pressure. At 0.15 MPa, 0.2 MPa, 0.25 MPa, 0.3 MPa, 0.35 MPa, and 0.4 MPa, the model calculated that grasping in the pipe was not possible

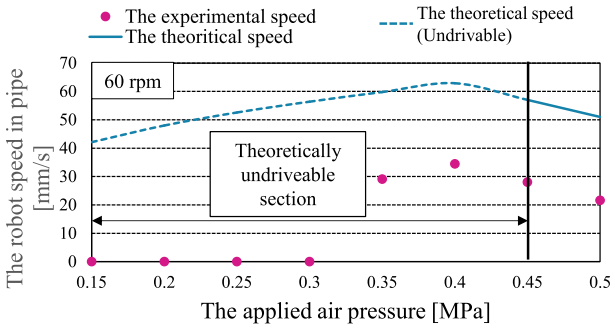

FIGURE 23. The relationship between robot speed and applied air pressure in 60 rpm. The dotted line indicates that the robot cannot run.

due to insufficient contraction and that running was not possible, but in the experiment, running was confirmed at 0.35 MPa and 0.4 MPa. At 0.45 MPa and 0.5 MPa, the experimental running speed was 50 % of the theoretical running speed. It was confirmed that each unit maintained its contraction and expansion state while running. We believe that the difference between the theoretical and experimental values is due to the fact that the artificial muscles are always in an inflated state, which inhibits the stretching motion and prevents them from fully extending forward.

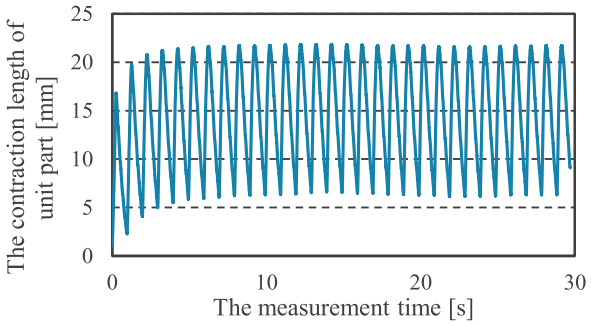

FIGURE 24. The relationship between contraction length and measurement time in 0.4 MPa, 60 rpm.

Therefore, we conducted an experiment to drive the unit for a long time in the same environment as PEW-RO V. The results are shown in Fig. 24, with a tube length of 1 m from the CRV to the unit. The model is designed only for the first time of repetitive driving of the artificial muscle and assumes that the CRV is directly connected to the artificial muscle. However, in the actual driving environment of the unit, as the rotation speed increases and the air tube length increases, the air discharge is delayed owing to the flow resistance and delay, and the residual pressure inside the unit accumulates. The results show that the artificial muscles contract and extend while maintaining their inflated state at high rotational speeds. As a result, it was confirmed that PEW-RO V could run in the pressure zone, which was calculated to be undriveable by this model.

Fig. 25 shows the theoretical values calculated by the model and the experimental values measured by the experiment for the traveling speed of the PEW-RO V in the pipe for

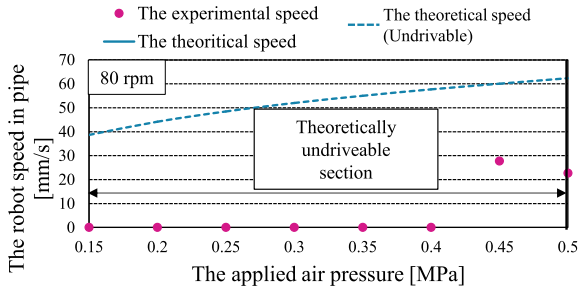

FIGURE 25. The relationship between robot speed and applied air pressure in 80 rpm. The dotted line indicates that the robot cannot run.

each applied pressure when the CRV was rotated at 80 rpm. The vertical axis shows the traveling speed of the robot, and the horizontal axis shows the applied pressure. At applied pressures of 0.15 MPa to 0.5 MPa, the model calculated that the robot could not grasp the pipe due to insufficient contraction and could not travel, but in the experiment, the robot traveled at pressures of 0.45 MPa and 0.5 MPa. We believe that this is because the PEW-RO V contracted and extended while maintaining the expansion state because of the accumulation of residual pressure caused by the high rotation speed drive, just as the PEW-RO V was able to travel even in the pressure zone where the model predicted that travel was impossible at 60 rpm.

VII. CONCLUSION

The aim of this study was to develop a pneumatic valve that can achieve a large periodic flow rate with a small and simple mechanism for a mobile robot in a pipe with periodic pneumatic actuation. We proposed a pneumatic valve based on the characteristics of a ball valve. As a wave propagation robot, the CRV was applied to a mobile in-pipe robot (PEW-RO V) developed by the authors in their previous study. The mechanical equilibrium model of the pneumatic actuators used in this study was also described. From this, it was confirmed that the PEW-RO V could be driven by reproducing the intended periodic motion by this valve through driving experiments. In addition, the flow rate of this valve is larger than that of the direct-acting solenoid valve drive system, confirming the effectiveness of this valve for wave propagation robots.

In the future, we will study the variation in the travel speed with respect to the rotation speed and applied pressure in the PEW-RO V system adopted in this study. Subsequently, we will study the application to other wave propagation robots driven by periodic motion.

REFERENCES

[1] *Key Messages*, Canadian Infrastructure Report Card, Canadian Urban Institute, 2019, p. 10. [Online]. Available: http://canadian infrastructure.ca/downloads/canadian-infrastructure-report-card-2019.pdf
[2] P. K. Dey, "A risk-based model for inspection and maintenance of cross-country petroleum pipeline," *J. Quality Maintenance Eng.*, vol. 7, no. 1, pp. 25–43, 2001, doi: 10.1108/13552510110386874.
[3] Q. Ma, G. Tian, Y. Zeng, R. Li, H. Song, Z. Wang, B. Gao, and K. Zeng, "Pipeline in-line inspection method, instrumentation and data management," *Sensors*, vol. 21, no. 11, p. 3862, Jun. 2021.

[4] J. A. I. Diaz, M. I. Ligeralde, M. A. B. Antonio, P. A. R. Mascardo, J. M. Z. Maningo, A. H. Fernando, R. R. P. Vicerra, E. P. Dadios, and A. A. Bandala, "Development of an adaptive in-pipe inspection robot with rust detection and localization," in *Proc. IEEE Region 10 Conf. (TENCON)*, Oct. 2018, pp. 2504–2509, doi: 10.1109/TENCON.2018.8650073.
[5] S.-G. Roh and H. R. Choi, "Differential-drive in-pipe robot for moving inside urban gas pipelines," *IEEE Trans. Robot.*, vol. 21, no. 1, pp. 1–17, Feb. 2005.
[6] B. Zhang, M. Abdulaziz, K. Mikoshi, and H. Lim, "Development of an in-pipe mobile robot for inspecting clefts of pipes," in *Proc. IEEE Int. Conf. Cybern. Intell. Syst. (CIS) IEEE Conf. Robot., Autom. Mechatronics (RAM)*, Nov. 2019, pp. 204–208, doi: 10.1109/CIS-RAM47153.2019.9095803.
[7] J. Min, Y. D. Setiawan, P. S. Pratama, S. B. Kim, and H. K. Kim, "Development and controller design of wheeled-type pipe inspection robot," in *Proc. Int. Conf. Adv. Comput., Commun. Informat. (ICACCI)*, Sep. 2014, pp. 789–795, doi: 10.1109/ICACCI.2014.6968543.
[8] C. Jun, Z. Deng, and S. Jiang, "Study of locomotion control characteristics for six wheels driven in-pipe robot," in *Proc. IEEE Int. Conf. Robot. Biomimetics*, Aug. 2004, pp. 119–124, doi: 10.1109/ROBIO.2004.1521762.
[9] K.-H. Yoon and Y.-W. Park, "Pipe inspection robot actuated by using compressed air," in *Proc. IEEE/ASME Int. Conf. Adv. Intell. Mechatronics*, Jul. 2010, pp. 1345–1349, doi: 10.1109/AIM.2010.5695865.
[10] F. Fukunaga and J.-Y. Nagase, "Cylindrical elastic crawler mechanism for pipe inspection inspired by amoeba locomotion," in *Proc. 6th IEEE Int. Conf. Biomed. Robot. Biomechatronics (BioRob)*, Jun. 2016, pp. 424–429, doi: 10.1109/BIOROB.2016.7523664.
[11] M. Ikeuchi, T. Nakamura, and D. Matsubara, "Development of an in-pipe inspection robot for narrow pipes and elbows using pneumatic artificial muscles," in *Proc. IEEE/RSJ Int. Conf. Intell. Robots Syst.*, Oct. 2012, pp. 926–931.
[12] X. Zhou, Y. Teng, and X. Li, "Development of a new pneumatic-driven earthworm-like soft robot," in *Proc. 23rd Int. Conf. Mechatronics Mach. Vis. Pract. (M2VIP)*, Nov. 2016, pp. 1–5, doi: 10.1109/M2VIP.2016.7827269.
[13] M. Kamata, S. Yamazaki, Y. Tanise, Y. Yamada, and T. Nakamura, "Development of pneumatically driven peristaltic-type robot for long distance inspection in half-inch pipes," in *Proc. IEEE Int. Conf. Adv. Intell. Mechatronics (AIM)*, Munich, Germany, Jul. 2017, pp. 309–314.
[14] J. Lim, H. Park, S. Moon, and B. Kim, "Pneumatic robot based on inchworm motion for small diameter pipe inspection," in *Proc. IEEE Int. Conf. Robot. Biomimetics (ROBIO)*, Dec. 2007, pp. 330–335, doi: 10.1109/ROBIO.2007.4522183.
[15] T. Takayama, H. Takeshima, T. Hori, and T. Omata, "A twisted bundled tube locomotive device proposed for in-pipe mobile robot," *IEEE/ASME Trans. Mechatronics*, vol. 20, no. 6, pp. 2915–2923, Dec. 2015.
[16] Y.-S. Kwon and B.-J. Yi, "Design and motion planning of a two-module collaborative indoor pipeline inspection robot," *IEEE Trans. Robot.*, vol. 28, no. 3, pp. 681–696, Jun. 2012, doi: 10.1109/TRO.2012.2183049.
[17] Y. Tanaka, K. Ito, T. Nakagaki, and R. Kobayashi, "Mechanics of peristaltic locomotion and role of anchoring," *J. Roy. Soc. Interface*, vol. 9, no. 67, pp. 222–233, Feb. 2012.
[18] T. Takayama and S. Hirose, "Amphibious 3D active cord mechanism 'HELIX' with helical swimming motion," in *Proc. IEEE/RSJ Int. Conf. Intell. Robots Syst.*, vol. 1, Sep./Oct. 2002, pp. 775–780, doi: 10.1109/IRDS.2002.1041484.
[19] K. Nakagawa, S. Dohta, T. Akagi, and W. Kobayashi, "Improvement of pipe holding mechanism for pipe inspection robot using flexible pneumatic cylinder," in *Proc. Int. Conf. Robot. Automat. Sci. (ICRAS)*, Aug. 2017, pp. 6–10.
[20] Z. Zhang, X. Wang, S. Wang, D. Meng, and B. Liang, "Design and modeling of a parallel-pipe-crawling pneumatic soft robot," *IEEE Access*, vol. 7, pp. 134301–134317, 2019.
[21] H. Tsukagoshi, K. Terashima, and Y. Takai, "A self-propelled catheter capable of generating travelling waves with steering function by mono-line drive," in *Proc. IEEE Int. Conf. Robot. Autom. (ICRA)*, May 2018, pp. 38–43, doi: 10.1109/ICRA.2018.8461159.
[22] A. Di Lallo, M. Catalano, M. Garabini, G. Grioli, M. Gabiccini, and A. Bicchi, "A novel approach to under-actuated control of fluidic systems," in *Proc. IEEE Int. Conf. Robot. Autom. (ICRA)*, May 2018, pp. 193–199, doi: 10.1109/ICRA.2018.8460859.
[23] T. Yamamoto, S. Sakama, and A. Kamimura, "Pneumatic duplex-chambered inchworm mechanism for narrow pipes driven by only two air supply lines," *IEEE Robot. Autom. Lett.*, vol. 5, no. 4, pp. 5034–5042, Oct. 2020, doi: 10.1109/LRA.2020.3003859.
[24] Y. Miyaki and H. Tsukagoshi, "Soft simple compact valve inducing self-excited vibration aimed for mobile robots unnecessary for electricity," in *Proc. IEEE/ASME Int. Conf. Adv. Intell. Mechatronics (AIM)*, Auckland, New Zealand, Jul. 2018, pp. 670–675.
[25] T. Takayama and Y. Sumi, "Self-excited air flow passage changing device for periodic pressurization of soft robot," *ROBOMECH J.*, vol. 8, no. 1, p. 20, Dec. 2021.
[26] G. Liang-bin and Z. Yun-xiang, "Calculation of the flow characteristics of a pipeline with an intermittent air source while considering the dynamic change of flow area of a ball valve," in *Proc. Int. Conf. Fluid Power Mechatronics (FPM)*, Harbin, China, Aug. 2015, pp. 1067–1071, doi: 10.1109/FPM.2015.7337275.
[27] H. Qiu, S. Dohta, T. Akagi, S. Shimooka, and S. Fujimoto, "Analytical model of pipe inspection robot using flexible pneumatic cylinder," in *Proc. 3rd Int. Conf. Intell. Technol. Eng. Syst. ICITES)* (Lecture Notes in Electrical Engineering), vol. 345, J. Juang, Ed. Cham, Switzerland: Springer, 2016, pp. 325–334, doi: 10.1007/978-3-319-17314-6_43.
[28] T. Tomita, T. Tanaka, and T. Nakamura, "Development of a peristaltic crawling robot for long-distance sewer pipe inspection with consideration of complex pipe line," in *Proc. IEEE/RSJ Int. Conf. Intell. Robots Syst. (IROS)*, Hamburg, Germany, Sep. 2015, pp. 2742–2747.
[29] T. Tanaka, K. Harigaya, and T. Nakamura, "Development of a peristaltic crawling robot for long-distance inspection of sewer pipes," in *Proc. IEEE/ASME Int. Conf. Adv. Intell. Mechatronics*, Besacon, France, Jul. 2014, pp. 1552–1557.
[30] R. Ishikawa, T. Tomita, Y. Yamada, and T. Nakamura, "Investigation of odometry method of pipe line shape by peristaltic crawling robot combined with inner sensor," in *Proc. IEEE Int. Conf. Adv. Intell. Mechatronics (AIM)*, Munich, Germany, Jul. 2017, pp. 1279–1284.
[31] Y. Mano, R. Ishikawa, Y. Yamada, and T. Nakamura, "Development of contraction force control system of peristaltic crawling robot for sewer pipe inspection," in *Proc. IEEE/ASME Int. Conf. Adv. Intell. Mechatronics (AIM)*, Auckland, New Zealand, Jul. 2018, pp. 936–941.
[32] Y. Mano, T. Yasui, Y. Yamada, and T. Nakamura, "Evaluation of running performance in a real environment of a peristaltic robot for inspection in a pumping pipe by field experiments," in *Proc. 20th SICE Syst. Integr. Division Lect.*, 2019, pp. 1365–1370.
[33] Y. Mano, R. Ishikawa, Y. Yamada, and T. Nakamura, "Development of high-speed type peristaltic crawling robot for long-distance and complex-line sewer pipe inspection," in *Proc. IEEE/RSJ Int. Conf. Intell. Robots Syst. (IROS)*, Madrid, Spain, Oct. 2018, pp. 8177–8183.
[34] H. Tomori and T. Nakamura, "Theoretical comparison of McKibben-type artificial muscle and novel straight-fiber-type artificial muscle," *Int. J. Autom. Technol.*, vol. 5, no. 4, pp. 544–550, Jul. 2011.
[35] T. Nakamura and H. Shinohara, "Position and force control based on mathematical models of pneumatic artificial muscles reinforced by straight glass fibers," in *Proc. IEEE Int. Conf. Robot. Autom.*, Roma, Italy, Apr. 2007, pp. 4361–4366.

HIROTO SATO received the B.S. degree from the Department of Precision Mechanics, Chuo University, Tokyo, Japan, in 2020, where he is currently pursuing the master's degree. His research interests include the research of miniaturization of pneumatic drive systems and self-position estimation.

KOUSUKE UCHIYAMA received the B.S. degree from the Department of Precision Mechanics, Chuo University, Tokyo, Japan, in 2021 where he is currently pursuing the master's degree. His research interest includes the development of a water suction system in a pipe.

YUKI MANO received the B.S. degree from the Department of Precision Mechanics, Chuo University, Tokyo, Japan, in 2018, where he is currently pursuing the master's degree. His research interest includes the research of miniaturization of pneumatic drive systems

FUMIO ITO (Graduate Student Member, IEEE) received the B.S and M.S. degrees from the Department of Precision Mechanics, Chuo University, Tokyo, Japan, in 2019 and 2021, respectively. He is currently pursuing the Ph.D. degree. His research interest includes the development of a biological robot based on the mantis shrimp.

SHUNICHI KURUMAYA received the B.S., M.S., and Ph.D. degrees from the Department of Mechanical Cosmology, Tokyo Institute of Technology, Tokyo, Japan, in 2015, 2016, and 2019, respectively. He was a Harvard University WYSS/SEAS Graduate Visiting Student, in 2016.

MANABU OKUI (Member, IEEE) received the B.S. and M.S. degrees in mechanical engineering from the Tokyo Institute of Technology, Tokyo, Japan, in 2012 and 2014, respectively. He joined Nissan Motor Company Ltd., in 2014. From 2016 to 2018, he was a Research Assistant with the Research and Develop Initiative, Chuo University, Tokyo. Since 2018, he has been an Assistant Professor with the Research and Develop Initiative, Chuo University.

YASUYUKI YAMADA (Member, IEEE) received the B.S., M.S., and Ph.D. degrees from Keio University, Japan, in 2009, 2011, and 2013, respectively. From 2013 to 2014, he was a Postdoctoral Researcher with the Tokyo Institute of Technology. He was also with Keio University. From 2014 to 2015, he was an Engineer at Nissan Motor Company Ltd. From 2015 to 2018, he was an Assistant Professor with Chuo University. He was also a Visiting Assistant Professor with the Dyson School of Design Engineering, Imperial College London, in 2018. In 2018, he joined Tokyo Denki University. In 2019, he joined Hosei University, where he is currently an Associate Professor with the Department of System Design Engineering.

TARO NAKAMURA (Member, IEEE) received the B.S. and M.S. degrees in mechanical engineering from Akita University, Akita, Japan, in 1997 and 1999, respectively, and the Ph.D. degree from Shinshu University, Nagano, Japan, in 2003. From 1999 to 2003, he was a Research Associate with Akita Prefecture University, Akita. In 2004, he was a Lecturer with the Faculty of Science and Engineering, Chuo University. From 2006 to 2013, he was an Associate Professor with Chuo University, Tokyo, Japan, where he has been a Professor, since 2013. From 2012 to 2013, he was a Visiting Professor with the Swiss Federal Institute of Technology Lausanne, EPFL, Lausanne, Switzerland.